

Low-Overhead Channel Estimation via 3D Extrapolation for TDD mmWave Massive MIMO Systems Under High-Mobility Scenarios

Binggui Zhou, Xi Yang, Shaodan Ma, Feifei Gao, and Guanghua Yang

Abstract—In time division duplexing (TDD) millimeter wave (mmWave) massive multiple-input multiple-output (MIMO) systems, the downlink channel state information (CSI) can be attained through uplink channel estimation thanks to the uplink-downlink channel reciprocity. However, the channel aging issue is significant under high-mobility scenarios and thus necessitates frequent uplink channel estimation. In addition, large amounts of antennas and subcarriers lead to high-dimensional CSI matrices, aggravating the pilot training overhead. To systematically reduce the pilot overhead, a spatial, frequency, and temporal domain (3D) channel extrapolation framework is proposed in this paper. Considering the marginal effects of pilots in the spatial and frequency domains and the effectiveness of traditional knowledge-driven channel estimation methods, we first propose a knowledge-and-data driven spatial-frequency channel extrapolation network (KDD-SFCEN) for uplink channel estimation by exploiting the least square estimator for coarse channel estimation and joint spatial-frequency channel extrapolation to reduce the spatial-frequency domain pilot overhead. Particularly, we propose the attention-based sub-element extrapolation module and the progressive extrapolation architecture to improve the accuracy of joint spatial-frequency channel extrapolation. Then, resorting to the uplink-downlink channel reciprocity and temporal domain dependencies of downlink channels, a temporal uplink-downlink channel extrapolation network (TUDCEN) is proposed for slot-level channel extrapolation, aiming to enlarge the pilot signal period and thus reduce the temporal domain pilot overhead under high-mobility scenarios. Specifically, we propose the spatial-frequency sampling embedding module to reduce the representation dimension and consequent computational complexity, and we propose to exploit the autoregressive generative Transformer for generating downlink channels autoregressively thanks to the powerful capability of generative artificial intelligence. Numerical results demonstrate the superiority of the proposed framework in significantly reducing the pilot training overhead by more than 16 times and improving the system's spectral efficiency under high-mobility scenarios.

Index Terms—Channel Extrapolation, High-Mobility Scenarios, Millimeter Wave, Uplink-Downlink Channel Reciprocity, Massive MIMO

I. INTRODUCTION

MILLIMETER wave (mmWave) massive multi-input multi-output (MIMO) has been recognized as a pivotal technology for the fifth generation (5G) wireless communication systems and beyond [1]–[3]. mmWave massive MIMO

is anticipated to provide spatial degrees of freedom, diversity or multiplexing gain, and array gain, thereby improving the spectral and energy efficiencies of wireless communication systems. To reap the benefits of massive MIMO, accurate channel state information (CSI) should be attained whether operating in the time division duplexing (TDD) or frequency division duplexing (FDD) modes [4], [5]. In FDD massive MIMO systems, the base station (BS) needs to obtain the downlink CSI through downlink channel estimation and CSI feedback from the user equipment (UE) due to the lack of uplink-downlink channel reciprocity. While in TDD massive MIMO systems, thanks to the uplink-downlink channel reciprocity, the BS can obtain the downlink CSI via uplink channel estimation and derive the downlink CSI from the estimated uplink CSI.

The uplink-downlink channel reciprocity in the TDD massive MIMO systems holds within the channel coherence time. However, in high-mobility scenarios, the channel is fast time-varying due to the UE movement, resulting in a short channel coherence time and the consequent channel aging issue, i.e., the channel varies between when it is acquired at the BS and when it is used for downlink precoding [6]. In addition, compared with sub-6 GHz bands, mmWave bands are more vulnerable to the UE movement since higher frequency bands generally lead to a shorter channel coherence time [7], deteriorating the channel aging issue in mmWave massive MIMO systems under high-mobility scenarios. To avoid significant performance degradation caused by channel aging, frequent channel estimation needs to be conducted such that the downlink precoding can be conducted based on up-to-date CSI, leading to huge temporal domain pilot training overhead. Besides, due to the large number of antennas at the BS and large amounts of subcarriers in orthogonal frequency-division multiplexing (OFDM) systems, the spatial and frequency domain pilot training overhead is also huge and unacceptable. In addition, to reduce the hardware cost and power consumption, hybrid beamforming structure is usually adopted and only a small number of radio frequency (RF) chains are deployed at the BS, especially for a millimeter wave (mmWave) massive MIMO system. To obtain the uplink CSI at all receiving antennas at the BS, the BS has to switch the antennas connected to these RF chains several times during the uplink channel estimation, leading to substantial time and power consumption. Therefore, it is of great significance to minimize the pilot training overhead in the spatial, frequency, and temporal domains while estimating the CSI accurately.

To circumvent huge frequency domain pilot training overhead, frequency domain channel extrapolation has been widely investigated in related works. In [8], a linear interpolation least square (LS) channel estimation method was proposed for channel estimation with pilots in partial subcarriers. In [9], the performance of various interpolation methods for mmWave MIMO-OFDM systems, including spline interpolation, discrete Fourier transform (DFT) -based

Binggui Zhou is with the School of Intelligent Systems Science and Engineering, Jinan University, Zhuhai 519070, China; and also with the State Key Laboratory of Internet of Things for Smart City and the Department of Electrical and Computer Engineering, University of Macau, Macao 999078, China (e-mail: binggui.zhou@connect.um.edu.mo).

Xi Yang is with the Shanghai Key Laboratory of Multidimensional Information Processing, School of Communication and Electronic Engineering, East China Normal University, Shanghai 200241, China (email: xyang@cee.ecnu.edu.cn).

Shaodan Ma is with the State Key Laboratory of Internet of Things for Smart City and the Department of Electrical and Computer Engineering, University of Macau, Macao 999078, China (e-mail: shaodanma@um.edu.mo).

Feifei Gao is with the Department of Automation, Tsinghua University, Beijing 100084, China (e-mail: feifeigao@ieee.org).

Guanghua Yang is with the School of Intelligent Systems Science and Engineering, Jinan University, Zhuhai 519070, China (e-mail: ghyang@jnu.edu.cn).

interpolation, etc., was investigated. Recently, with the advances in deep learning, many deep learning-based frequency domain channel extrapolation methods were proposed to further reduce pilot training overhead and improve channel estimation accuracy from the frequency domain perspective. In [10], the super-resolution convolutional neural network (SRCNN) was presented to obtain full channel responses with the channel responses at pilot positions via deep image processing techniques. By jointly learning the spatial-temporal domain features of massive MIMO channels with a temporal attention module and a spatial attention module, a dual-attention-based channel estimation network (DACEN) was proposed to realize accurate channel estimation via low-density pilots in the frequency domain [11].

The development of deep learning has also led to increasing attention in antenna (spatial) domain channel extrapolation in recent years, aiming at reducing the huge spatial domain pilot training overhead and prohibitive time and power consumption. For example, two fully connected neural networks (FCNNs) were proposed to use the CSI of a subset of antennas to extrapolate the CSI of other antennas [12], [13].

In addition to spatial and frequency domain channel extrapolation, channel prediction (i.e., temporal domain channel extrapolation) is also a convincing method for alleviating the huge pilot training overhead in high-mobility scenarios. Linear extrapolation methods [14] and statistical prediction models, e.g., autoregressive (AR) models [15], [16], were proposed and have demonstrated that channel prediction is promising to mitigate the impacts of channel aging. The advancements of DNNs further improve the channel prediction performance and thus would further reduce the channel estimation frequency in high-mobility scenarios. In [17], a novel long short-term memory (LSTM) based channel predictor was proposed to learn channel variations and thereby reduce the pilot training overhead for channel estimation. An attention-based channel predictor was proposed in [18] to achieve frame-level channel estimates for mobile scenarios. Nonetheless, existing channel prediction methods are unable to deal with massive MIMO-OFDM systems with substantial antennas and subcarriers due to the high-dimensional CSI matrices and the consequent tremendous computational complexity. In addition, since the channel aging issue is critical in high-mobility scenarios, frame-level channel prediction methods are unable to achieve high spectral efficiency due to the varying channels, posing demands on slot-level channel extrapolation. However, existing channel prediction methods predict future channels at the same time granularity as the collected historical channels. This indicates that exploiting these methods for slot-level channel extrapolation comes at the cost of sacrificing a large amount of time-frequency resources for slot-level historical channel estimation, making them infeasible in practice.

To overcome the limitations of these existing works and to systematically reduce the pilot overhead, a spatial, frequency, and temporal domain (3D) channel extrapolation framework is proposed in this paper to reduce the pilot training overhead from these three domains respectively. First, it can be observed that the number of pilots in one certain domain shows the marginal effect, i.e., as the number of pilots in this domain increases, the improvement in channel estimation accuracy gradually decreases.¹ Due to the capability of deep neural networks (DNNs) in extracting

the spatial and frequency domain characteristics of massive MIMO channels, it is expected that exploiting DNNs for joint spatial and frequency domain channel extrapolation will further reduce the pilot training overhead. However, although some works have pointed out that jointly learning spatial-frequency domain features is beneficial to channel estimation [11], [19], spatial-frequency channel extrapolation has not yet been well investigated to reduce the pilot training overhead for mmWave massive MIMO-OFDM systems. Therefore, considering the marginal effects of pilots in the spatial and frequency domains and the effectiveness of traditional knowledge-driven channel estimation methods, we first propose a knowledge-and-data driven spatial-frequency channel extrapolation network (KDD-SFCEN) for uplink channel estimation by exploiting the least square estimator for coarse channel estimation and joint spatial-frequency channel extrapolation to reduce the spatial-frequency domain pilot overhead. Then, resorting to the uplink-downlink channel reciprocity and temporal domain dependencies of downlink channels, a temporal uplink-downlink channel extrapolation network (TUDCEN) is proposed for slot-level channel extrapolation, aiming to enlarge the pilot signal period and thus reduce the temporal domain pilot overhead. To the best of our knowledge, none of the existing works have investigated such a systematic framework to reduce the pilot training overhead and improve the spectral efficiency of mmWave massive MIMO-OFDM systems under high-mobility scenarios. The major contributions of this paper are summarized as follows:

- 1) We propose the KDD-SFCEN to reduce the spatial-frequency domain pilot overhead effectively via joint spatial-frequency channel extrapolation. In addition, it is worth emphasizing that the substantial time and power consumption due to antenna switching can be avoided through spatial extrapolation. The proposed KDD-SFCEN consists of a knowledge-driven coarse channel estimator to provide coarse channel estimates and accelerate the training of the proposed network. The KDD-SFCEN also comprises a spatial-frequency channel extrapolator encompassing the attention-based sub-element extrapolation module and the progressive extrapolation architecture. The proposed attention-based sub-element extrapolation module mimics the sub-pixel imaging technology and is demonstrated to be highly effective in learning spatial-frequency channel characteristics for joint spatial and frequency extrapolation. Moreover, the progressive extrapolation architecture is proposed to progressively extrapolate the uplink CSI, thereby further improving the performance of joint spatial-frequency channel extrapolation with few pilots in the spatial and frequency domains.
- 2) We propose the TUDCEN for accurate slot-level channel extrapolation given the estimated uplink CSI at the first slot. Through the proposed TUDCEN, channel estimation can be conducted less frequently and more slots can be configured for data transmission under high-mobility scenarios, further reducing the pilot training overhead from the temporal domain perspective and improving the system's spectral efficiency. The TUDCEN is composed of an uplink-downlink channel calibration network (UDCCN) and a downlink channel extrapolation network (DCEN). The UDCCN calibrates the estimated uplink channel to the downlink channel at the first downlink slot to compensate for the hardware asymmetry in transceivers. The proposed DCEN achieves slot-level channel extrapolation via spatial-frequency

¹This observation is further validated with our simulation results in Section V-B.

sampling embedding and autoregressive generation with the generative Transformer [20]. Spatial-frequency sampling embedding is proposed to reduce the tremendous computational complexity due to high-dimensional CSI matrices. Specifically, the spatial-frequency sampling embedding layer samples the spatial and frequency domain representation of downlink channels with a spatial sampling factor and a frequency sampling factor to reduce the representation dimension by resorting to the spatial and frequency correlations of downlink channels. Meanwhile, the sampled antenna groups and subcarrier groups are combined to facilitate model training. We exploit the generative Transformer for generating downlink channels autoregressively thanks to the powerful capability of generative artificial intelligence (AI), which is able to conduct slot-level downlink channel extrapolation given only the first downlink channel, thereby avoiding heavy slot-level historical downlink channel estimation.

- 3) We use the sounding reference signal (SRS) defined by the 3rd generation partnership project (3GPP) 5G technical specification [21] as the pilot signal for uplink pilot training. The frame structures and system settings in framework design and numerical simulations also follow the 3GPP 5G technical specification. Numerical results demonstrate the superiority of the proposed framework in significantly reducing the spatial-frequency domain pilot overhead by more than 4 times via spatial-frequency channel extrapolation. In addition, via enlarging the pilot signal period with slot-level channel extrapolation, the proposed framework further reduces the temporal domain pilot overhead by 4 times and significantly improves the mmWave massive MIMO system's spectral efficiency under high-mobility scenarios.

The remainder of this paper is organized as follows. In Section II, we introduce the system model and formulate the spatial, frequency, and temporal channel extrapolation problem. In Section III, we propose the KDD-SFCEN for uplink channel estimation to reduce the spatial-frequency domain pilot training overhead. In Section IV, we propose the TUDCEN for slot-level channel extrapolation to enlarge the pilot signal period and thus reduce the temporal domain pilot overhead. In Section V, simulation results are presented to demonstrate the superiority of the proposed spatial, frequency, and temporal channel extrapolation framework. Finally, we conclude this work in Section VI.

Notation: Underlined bold uppercase letter $\underline{\mathbf{A}}$, bold uppercase letter \mathbf{A} , and bold lowercase letter \mathbf{a} represent a tensor, a matrix, and a vector, respectively. Calligraphy uppercase letter \mathcal{A} represents a set. $\mathbf{A}\{s, t\}$ denotes the representation of \mathbf{A} at the t -th slot of the s -th sub-frame. $\mathbf{A}_{:,n}$ and $\mathbf{A}_{m,:}$ denote the n -th column and the element at the m -th row and n -th column of the matrix \mathbf{A} , respectively. $(\cdot)^T$, $(\cdot)^H$, and $(\cdot)^{-1}$ denote the transpose, conjugate-transpose, and inverse of a matrix, respectively. $\lceil \cdot \rceil$, \odot , $\mathbb{E}\{\cdot\}$, and $\|\cdot\|_2$ denote the ceiling function, Hadamard product, expectation, and L2 norm, respectively.

II. SYSTEM MODEL AND PROBLEM FORMULATION

A. System Model

As shown in Fig. 1 (a), we consider a mmWave massive MIMO system working in the TDD mode, where a single BS equipped with $N_T \gg 1$ antennas and $N_{RF} \ll N_T$ RF chains serves a single user equipped with N_R antennas. The

BS is realized with a hybrid precoding architecture, as Fig. 1 (b) shows. The system operates with the OFDM modulation with a total of $N_c \gg 1$ subcarriers. By leveraging the uplink-downlink channel reciprocity in the TDD system, the downlink channel can be acquired via uplink channel estimation to avoid downlink channel estimation and feedback at the UE side, thereby improving the system's spectral efficiency. A simplified downlink CSI acquisition and data transmission process based on uplink pilot training is also shown in Fig. 1 (a). The process consists of three phases, i.e., uplink pilot transmission (phase 1), BS signal processing (phase 2), and downlink data transmission (phase 3). Specifically, the uplink pilot signal is first transmitted by the UE to the BS for uplink channel estimation (phase 1). Then the BS estimates the uplink channel given the received pilot signal, derives the downlink channel, and conducts downlink precoding (phase 2). After that, the BS transmits data symbols to the UE based on the downlink precoder and other transmission parameters (phase 3).

Due to the limited number of RF chains, only the uplink CSI at N_{RF} antennas connected to the N_{RF} RF chains can be obtained in each uplink pilot signaling process. Therefore, to obtain the uplink CSI at all N_T antennas, the BS has to switch the antennas connected to these N_{RF} RF chains for $\frac{N_T}{N_{RF}}$ times, leading to huge time and power consumption. Specifically, for the i -th subcarrier and the k -th uplink pilot signaling process, denote the uplink CSI at N_{RF} antennas, the transmitted diagonal pilot signal, the received pilot signal, and the uplink noise as $\mathbf{H}_i^{(k)} \in \mathbb{C}^{N_{RF} \times N_R}$, $\mathbf{S}_i^{p(k)} \in \mathbb{C}^{N_{RF} \times N_{RF}}$, $\mathbf{Y}_i^{p(k)} \in \mathbb{C}^{N_{RF} \times N_{RF}}$, and $\mathbf{N}_i^{p(k)} \in \mathbb{C}^{N_{RF} \times N_{RF}}$, respectively. The set of antennas connected to RF chains in the k -th uplink pilot signaling process is denoted as $\mathcal{A}_{RF}^{(k)}$, and $\mathbf{H}_i^{(k)}$ corresponds to the uplink CSI at antennas in $\mathcal{A}_{RF}^{(k)}$. Then, $\mathbf{Y}_i^{p(k)}$ can be represented as

$$\mathbf{Y}_i^{p(k)} = \mathbf{H}_i^{(k)} \mathbf{S}_i^{p(k)} + \mathbf{N}_i^{p(k)}, \quad (1)$$

where $\mathbf{H}_i^{(k)}$ can then be estimated by a channel estimator f_{uce} given $\mathbf{Y}_i^{p(k)}$ and $\mathbf{S}_i^{p(k)}$ as

$$\hat{\mathbf{H}}_i^{(k)} = f_{uce}(\mathbf{Y}_i^{p(k)}, \mathbf{S}_i^{p(k)}), \quad (2)$$

where $\hat{\mathbf{H}}_i^{(k)} \in \mathbb{C}^{N_{RF} \times N_R}$ is the estimate of $\mathbf{H}_i^{(k)}$. By repeating the uplink pilot signaling process for $\frac{N_T}{N_{RF}}$ times, the uplink channel at the i -th subcarrier, i.e., $\mathbf{H}_i \in \mathbb{C}^{N_T \times N_R}$, can be obtained as

$$\hat{\mathbf{H}}_i = [(\hat{\mathbf{H}}_i^{(1)})^T, \dots, (\hat{\mathbf{H}}_i^{(k)})^T, \dots, (\hat{\mathbf{H}}_i^{(\frac{N_T}{N_{RF}})})^T]^T, \quad (3)$$

where $\hat{\mathbf{H}}_i$ is the estimate of \mathbf{H}_i , and

$$\mathcal{A} = \mathcal{A}_{RF}^{(1)} \cup \dots \cup \mathcal{A}_{RF}^{(k)} \cup \dots \cup \mathcal{A}_{RF}^{(\frac{N_T}{N_{RF}})}, \quad (4)$$

where \mathcal{A} is the set containing all BS antennas. Then, due to the hardware asymmetry in transceivers [22], the downlink channel at the i -th subcarrier, i.e., $\mathbf{H}_i^d \in \mathbb{C}^{N_R \times N_T}$, has to be derived from $\hat{\mathbf{H}}_i$ based on the uplink-downlink channel reciprocity and via channel calibration as

$$\hat{\mathbf{H}}_i^d = f_c(\hat{\mathbf{H}}_i), \quad (5)$$

where $\hat{\mathbf{H}}_i^d \in \mathbb{C}^{N_R \times N_T}$ is the estimate of \mathbf{H}_i^d , and $f_c(\cdot)$ denotes the uplink-downlink channel calibration function.

Given $\hat{\mathbf{H}}_i^d$, the downlink precoding matrix $\mathbf{F}_i \in \mathbb{C}^{N_T \times N_s}$ at the i -th subcarrier with N_s being the number of data streams and $N_s \leq N_R$ can be designed by the singular value decomposition (SVD)-based precoding algorithm [23]. Specifically, SVD for $\hat{\mathbf{H}}_i^d$ can be expressed as

$$\hat{\mathbf{H}}_i^d = \mathbf{U}_i \mathbf{\Sigma}_i \mathbf{V}_i^H, \quad (6)$$

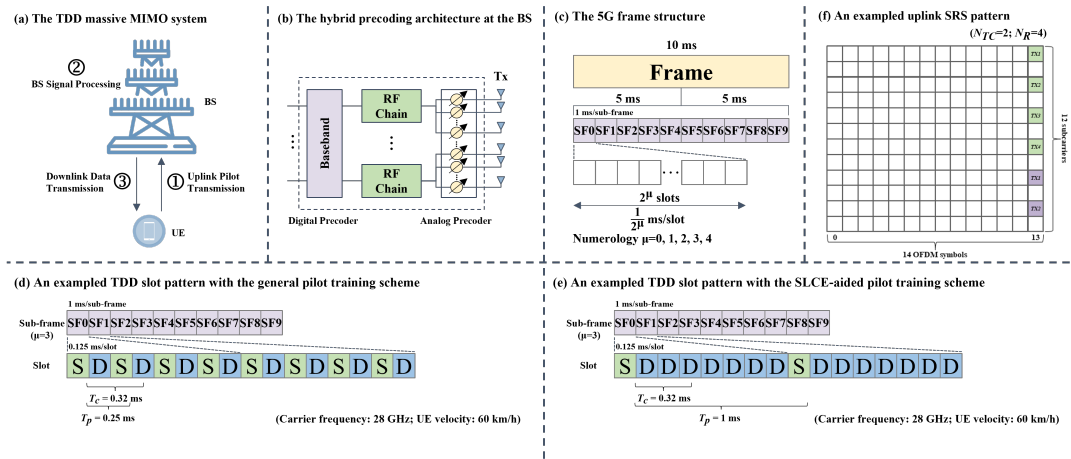


Fig. 1. A TDD massive MIMO system with the hybrid precoding architecture at the BS. (a) The TDD massive MIMO system; (b) The hybrid precoding architecture at the BS; (c) The 5G frame structure; (d) An exemplified TDD slot pattern with a general pilot training scheme; (e) An exemplified TDD slot pattern with the SLCE-aided pilot training scheme; (f) An exemplified uplink SRS pattern.

where $\mathbf{U}_i \in \mathbb{C}^{N_R \times N_R}$, $\mathbf{\Sigma}_i \in \mathbb{C}^{N_R \times N_T}$, and $\mathbf{V}_i^H \in \mathbb{C}^{N_T \times N_T}$ are the left singular vectors matrix, the diagonal matrix of singular values, and the right singular vectors matrix, respectively. Note that $\mathbf{F}_i = [\mathbf{f}_i^{(1)}, \mathbf{f}_i^{(2)}, \dots, \mathbf{f}_i^{(N_s)}]$, where $\mathbf{f}_i^{(j)} \in \mathbb{C}^{N_T \times 1}$, $j = 1, 2, \dots, N_s$ are the first N_s column vectors of \mathbf{V} . Then, in the downlink transmission, the received signal $\mathbf{y}_i \in \mathbb{C}^{N_R \times 1}$ at the i -th subcarrier can be represented as

$$\mathbf{y}_i = \mathbf{H}_i^d \mathbf{F}_i \mathbf{s}_i + \mathbf{n}_i, \quad (7)$$

where $\mathbf{s}_i \in \mathbb{C}^{N_s \times 1}$ and $\mathbf{n}_i \in \mathbb{C}^{N_s \times 1}$ are the transmitted signal and the downlink noise at the i -th subcarrier, respectively.

B. Problem Formulation

To support the measurement of all transmit ports and subcarriers, the length of the pilot signal is $N_R \times N_c$. Therefore, the pilot training overhead is $(N_{RF} \times \frac{N_T}{N_{RF}}) \times N_R \times N_c = N_T \times N_R \times N_c$. Considering a large number of antennas and subcarriers in the system, the pilot training overhead is extremely high and significantly challenging to the system's spectral efficiency. In addition, the time and power consumption due to the switching of antennas connected to RF chains is also unaffordable. Moreover, the pilot signal should be transmitted for uplink channel estimation every channel coherence time T_c to avoid significant channel aging. For simplicity, we call this scheme the general pilot training scheme hereafter. We denote the pilot signal period as T_p and for the general pilot training scheme we have $T_p \leq T_c$. Note that as specified in the 3GPP 5G technical specification [21], the frame structure in the 5G new radio (NR) is shown in Fig. 1 (c). Each frame spans 10 ms and is divided into two half-frames. Each half-frame spans 5 ms and contains five sub-frames, with each sub-frame spanning 1 ms. The number of slots in one sub-frame, i.e., N_{slot} , is determined by the numerology μ , and $N_{slot} = 2^\mu$. Here we assume $\mu = 3$ which indicates $N_{slot} = 8$ in one sub-frame and each slot spans 0.125 ms. It should be emphasized that under scenarios with high carrier frequency and high UE mobility, the channel coherence time could be very short. For instance, when operating at a carrier frequency of 28 GHz and with the UE velocity of 60 km/h, the channel coherence time is approximately 0.32 ms [18]. With the general pilot training scheme, the TDD slot pattern can be illustrated by Fig. 1 (d), where 'S' stands for a special slot configured for uplink channel estimation and 'D' stands for a downlink

slot for downlink data transmission.² The pilot signal has to be transmitted every two slots (i.e., $T_p = 0.25$ ms) to mitigate channel aging with $T_c = 0.32$ ms, further degrading the system's spectral efficiency.³

Defining the single-slot pilot training overhead C_{sl} as the pilot training overhead for one-time uplink channel estimation (i.e., the spatial-frequency domain pilot overhead), the overall pilot training overhead C_o for an interval of length T is defined as

$$C_o \triangleq \frac{T}{T_p} \times C_{sl}. \quad (8)$$

From the previous discussions, the overall pilot training overhead C_o is huge, since the single-slot pilot training overhead C_{sl} is large due to the high-dimensional CSI matrices and the pilot signal period T_p is short in high-mobility scenarios. To circumvent such huge overall pilot training overhead, we consider spatial, frequency, and temporal channel extrapolation to systematically reduce the pilot training overhead from two perspectives: 1) reducing the single-slot pilot training overhead C_{sl} (i.e., the spatial-frequency domain pilot overhead) via spatial-frequency channel extrapolation; 2) enlarging the pilot signal period T_p via slot-level channel extrapolation and thereby reducing the temporal domain pilot overhead. In addition, it is worth noting that through spatial extrapolation, the substantial time and power consumption due to antenna switching can be avoided. And through the slot-level channel extrapolation, more slots can be configured for data transmission to improve the system's spectral efficiency. The overall framework of the proposed method is shown in Fig. 2.

On the one hand, considering the marginal effects of pilots in the spatial and frequency domains, spatial channel extrapolation and frequency channel extrapolation are combined to reduce the single-slot pilot training overhead C_{sl} and circumvent the time and power consumption during single-slot uplink channel estimation (SSUCE). Specifically, the N_{RF} RF chains are connected to N_{RF} uniformly sampled antennas out of all N_T antennas without antenna switching in the whole uplink channel estimation phase, and the pilot symbols are configured only on partial subcarriers. Ultimately, only the partial uplink CSI can be obtained directly from

²Note that for ease of elaboration, we do not consider uplink data transmission slots in the sub-frame. Our method can be easily extended to sub-frames with uplink data transmission slots.

³Note that in Fig. 1 (d), (e), and (f), we assume the pilot symbol is configured at the last symbol index of each special slot.

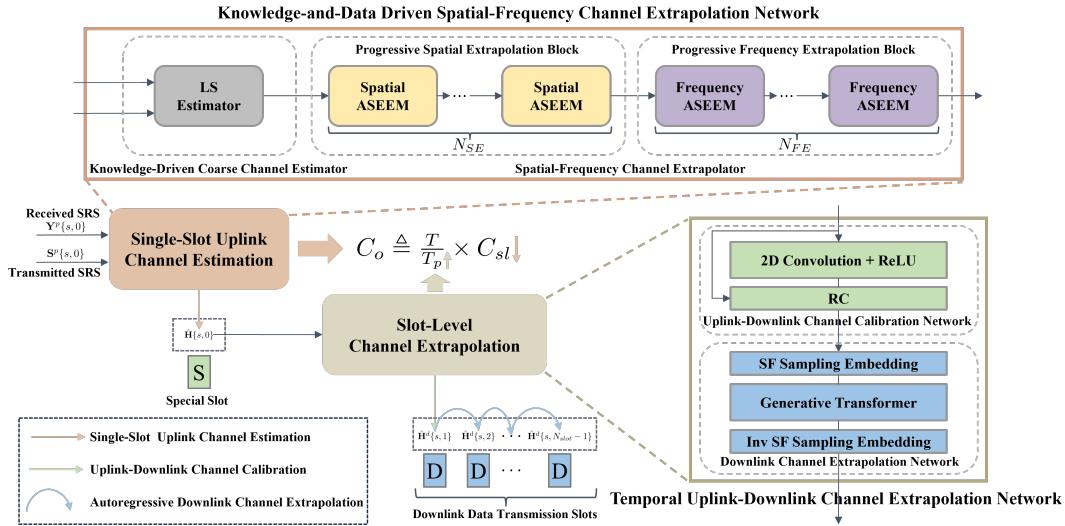


Fig. 2. The overall framework of the proposed spatial, frequency, and temporal channel extrapolation method. The proposed method first realizes uplink channel estimation with the KDD-SFCEN to reduce the spatial-frequency domain pilot training overhead C_{sl} , and then conducts accurate slot-level channel extrapolation to enlarge the pilot signal period T_p with the TUDCEN, thereby systematically reducing the pilot training overhead C_o .

the received pilot signal, and then the full uplink CSI is extrapolated from the partial uplink CSI. Denote the transmitted diagonal pilot signal matrix and the corresponding received pilot signal matrix by $\mathbf{S}^p \in \mathbb{C}^{(N_R \times N'_c) \times (N_R \times N'_c)}$ and $\mathbf{Y}^p \in \mathbb{C}^{N_{RF} \times (N_R \times N'_c)}$, respectively, where N'_c is the number of subcarriers configured with pilot symbols. In addition, by concatenating \mathbf{H}_i , $i = 1, 2, \dots, N_c$, the uplink channel at all subcarriers, denoted by $\mathbf{H} \in \mathbb{C}^{N_T \times (N_R \times N_c)}$, can be given by:

$$\mathbf{H} = [\mathbf{H}_1, \mathbf{H}_2, \dots, \mathbf{H}_{N_c}]. \quad (9)$$

Further denoting $\mathbf{H}\{s, t\} \in \mathbb{C}^{N_T \times (N_R \times N_c)}$, $\mathbf{S}^p\{s, t\} \in \mathbb{C}^{(N_R \times N'_c) \times (N_R \times N'_c)}$, and $\mathbf{Y}^p\{s, t\} \in \mathbb{C}^{N_{RF} \times (N_R \times N'_c)}$ as the uplink channel, the transmitted diagonal pilot signal matrix, and the received pilot signal matrix at the t -th slot of the s -th sub-frame, respectively, the uplink channel at the first slot of the s -th sub-frame can be estimated based on spatial-frequency channel extrapolation as

$$\hat{\mathbf{H}}\{s, 0\} = F_{ssuce}(\mathbf{Y}^p\{s, 0\}, \mathbf{S}^p\{s, 0\}), \quad (10)$$

where $\hat{\mathbf{H}}\{s, 0\}$ is the estimate of $\mathbf{H}\{s, 0\}$, and F_{ssuce} is a DNN-based SSUCE model.

On the other hand, we propose to enlarge the pilot signal period T_p by leveraging the uplink-downlink channel reciprocity and temporal dependencies for slot-level channel extrapolation (SLCE). In TDD systems, it is commonly assumed that the uplink and downlink channels are reciprocal during the channel coherence time, such that the downlink channel can be derived from the estimated uplink channel. Note that due to high UE mobility and short channel coherence time, the uplink-downlink channel reciprocity only holds for the special slot of a sub-frame and a few downlink data transmission slots in the same sub-frame. And due to the hardware asymmetry in transceivers, uplink-downlink channel calibration is required to derive the downlink channel accurately from the estimated uplink channel. Moreover, like many real-world phenomena, wireless channels exhibit temporal dependencies over time (e.g., explicit patterns like trends, etc). Capturing these temporal dependencies from downlink channels allows us to conduct accurate temporal extrapolation for future slots. However, the temporal dependencies for high-dimensional channels are challenging to capture. Fortunately, with DNNs, it is promising to learn the uplink-downlink channel reciprocity and temporal dependencies for

SLCE. Then, with SLCE, the pilot signal can be transmitted with a pilot signal period $T_p \gg T_c$. Taking transmitting the pilot signal only once per sub-frame and at the first slot of each sub-frame as an example, the TDD slot pattern with the SLCE-aided pilot training scheme is provided in Fig. 1 (e).⁴ In this example, the pilot signal period is $T_p = 1$ ms, which is much larger than the channel coherence time $T_c = 0.32$ ms. To tackle the channel aging issue caused by high carrier frequency and high UE mobility, SLCE is thus anticipated to predict the downlink channels within the pilot signal period accurately for downlink data transmission. Specifically, based on the estimated uplink channel at the special slot, the downlink channel at the first downlink data transmission slot can be initially acquired by exploiting the uplink-downlink channel reciprocity and via channel calibration. Then, by learning the temporal dependencies among time-varying downlink channels, accurate estimates of the downlink channels at all other downlink data transmission slots can be achieved. Therefore, denoting $\mathbf{H}^d\{s, t\} \in \mathbb{C}^{N_R \times (N_T \times N_c)}$ as the downlink channel at the t -th slot of the s -th sub-frame, the SLCE problem can be formulated as

$$\hat{\mathbf{H}}^d\{s, 1\}, \dots, \hat{\mathbf{H}}^d\{s, N_{slot} - 1\} = F_{slce}(\hat{\mathbf{H}}\{s, 0\}), \quad (11)$$

where $\hat{\mathbf{H}}^d\{s, t\}$ is the estimate of $\mathbf{H}^d\{s, t\}$, F_{slce} is a DNN-based SLCE model.

C. Sounding Reference Signal Pattern

Following the 3GPP technical specification [21], the sounding reference signal (SRS) is used as the pilot signal for uplink pilot training. The SRS is configured according to the transmission comb number N_{TC} in the frequency domain and with frequency domain code division multiplexing (fd-CDM) for multiple antenna ports. For example, assuming the transmission comb number $N_{TC} = 2$ and the UE antenna number $N_R = 4$, the uplink SRS pattern in one resource block (RB) can be illustrated by Fig. 1 (f), where the SRS is configured with every other resource element (RE) and has an fd-CDM length of 4 to support 4 UE antennas. Based on N_{TC} and the number of RBs, i.e., N_{RB} , the received pilot signal matrix \mathbf{Y}^p is with the size of $N_{RF} \times (N_R \times N'_c) =$

⁴Note that for ease of elaboration, in the following context, we simply use this TDD slot pattern and suppose the pilot signal only once per sub-frame. The pilot signal can be set flexibly in practice.

$N_{RF} \times (N_R \times N_{RB} \times \frac{12}{N_{TC}})$, where 12 is the number of consecutive subcarriers that form a RB as defined in [21]. Therefore, compared with the size of the uplink channel \mathbf{H} , i.e., $N_T \times (N_R \times N_c) = N_T \times (N_R \times N_{RB} \times 12)$, we define the spatial compression ratio as $R_s = \frac{N_T}{N_{RF}}$ and the frequency compression ratio as $R_f = N_{TC}$.

In the following two sections, to reduce the overall pilot training overhead C_o from the aforementioned two perspectives, i.e., reducing the single-slot pilot training overhead C_{sl} and enlarging the pilot signal period T_p , we propose the KDD-SFCEN for single-slot uplink channel estimation and the TUDCEN for slot-level channel extrapolation respectively.

III. SPATIAL-FREQUENCY CHANNEL EXTRAPOLATION BASED SINGLE-SLOT UPLINK CHANNEL ESTIMATION

Considering the marginal effects of pilots in the spatial and frequency domains, we propose to conduct joint spatial-frequency channel extrapolation to reduce the pilot training overhead of single-slot uplink channel estimation. Traditional channel estimation methods based on domain knowledge have been fully validated for decades that they can provide feasible channel estimates in time-invariant channels, which can be exploited as initial estimates for deep learning-based channel estimation methods. In addition, to estimate the uplink channel accurately with only a few pilots in both the spatial and frequency domains, the spatial and frequency characteristics of massive MIMO channels must be fully exploited [11]. Therefore, in this section, we propose the KDD-SFCEN for single-slot uplink channel estimation in TDD massive MIMO systems, which benefits from both domain knowledge via the traditional knowledge-driven channel estimation and data via joint spatial-frequency channel extrapolation. As shown in Fig. 2, the proposed network consists of two components, i.e., a knowledge-driven coarse channel estimator and a spatial-frequency channel extrapolator, for coarse channel estimation and spatial-frequency channel extrapolation, respectively.

A. Coarse Channel Estimation

Since traditional LS estimation has been demonstrated to be a simple but effective method to achieve coarse channel estimates, we exploit this domain knowledge and use the traditional LS estimator as the knowledge-driven coarse channel estimator to accelerate the training of our proposed uplink channel estimation network. Specifically, the received pilot signal $\mathbf{Y}^p\{s, 0\}$ and the corresponding transmitted diagonal pilot signal $\mathbf{S}^p\{s, 0\}$ is first processed by an LS estimator as

$$\hat{\mathbf{H}}^{LS} = \mathbf{Y}^p\{s, 0\} \{\mathbf{S}^p\{s, 0\}\}^{-1}, \quad (12)$$

where $\hat{\mathbf{H}}^{LS} \in \mathbb{C}^{N_{RF} \times (N_R \times N_c)}$ is the coarse channel estimate achieved by the knowledge-driven coarse channel estimator.

Then, the coarse channel estimate is further extrapolated and refined by the spatial and frequency channel extrapolator to achieve a highly accurate channel estimate.

B. Spatial and Frequency Channel Extrapolation

To estimate the uplink channel accurately with a few pilots, we propose the attention-based sub-element extrapolation module (ASEEM) to fully exploit the spatial and frequency characteristics of massive MIMO channels. In addition, directly extrapolating partial CSI to full CSI is significantly challenging, especially when the spatial and frequency compression ratios are large. Therefore, we propose to conduct

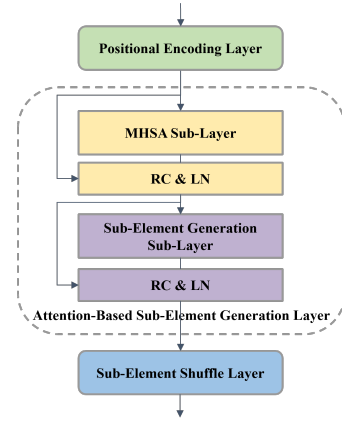


Fig. 3. The architecture of the proposed ASEEM.

spatial and frequency channel extrapolation progressively. As Fig. 2 shows, the proposed spatial-frequency channel extrapolator consists of a progressive spatial extrapolation block and a progressive frequency extrapolation block for spatial and frequency extrapolation, respectively. The progressive spatial extrapolation block and the progressive frequency extrapolation block consist of N_{SE} spatial ASEEMs and N_{FE} frequency ASEEMs, respectively. These spatial/frequency ASEEMs progressively extrapolate partial spatial/frequency CSI to full spatial/frequency CSI.

1) *ASEEMs*: Partial CSI in either the spatial or frequency domain can be regarded as downsampled information from full CSI in the specific domain, which is similar to an image taken from the real world. Generally, a pixel is the smallest addressable element of an image. However, a pixel in an image might correspond to many small objects in the real world. Motivated by this, sub-pixel imaging technologies emerge by dividing a single pixel into smaller sub-pixels to improve the resolution of an image. Similarly, learning to divide each element in a partial CSI into smaller sub-elements will facilitate CSI extrapolation. This motivates us to propose the ASEEM, which is composed of one positional encoding layer, one attention-based sub-element generation layer, and one sub-element shuffle layer. To better illustrate the proposed ASEEM, the architecture of the ASEEM is provided in Fig. 3.

Denote the input to the ASEEM as $\mathbf{X} \in \mathbb{R}^{N_I \times d_R}$, where N_I is the number of initial input elements and d_R is the representation dimension of each input element. The positional encoding layer generates a positional encoding (PE) $\mathbf{P} \in \mathbb{R}^{N_I \times d_R}$ for all input elements of \mathbf{X} as

$$\mathbf{P} = \text{Embed}(\mathbf{p}^{idx}; \Theta^P), \quad (13)$$

$$\mathbf{p}^{idx} = [1, 2, \dots, N_I], \quad (14)$$

where $\mathbf{p}^{idx} \in \mathbb{R}^{N_I \times 1}$ is the positional index vector to all input elements, $\text{Embed}(\cdot)$ is the embedding function parameterized by $\Theta^P \in \mathbb{R}^{N_I \times d_R}$ that converts the positional index vector \mathbf{p}^{idx} into the learnable positional encoding \mathbf{P} . Then, the input to the attention-based sub-element generation layer, denoted by $\tilde{\mathbf{X}} \in \mathbb{R}^{N_I \times d_R}$ can be obtained by

$$\tilde{\mathbf{X}} = \mathbf{X} + \mathbf{P}. \quad (15)$$

The attention-based sub-element generation layer further consists of one multi-head self-attention (MHSA) sub-layer, one sub-element generation (SEG) sub-layer, and residual connection (RC) [24] and layer normalization (LN) [25] operations around each of the two sub-layers. By splitting the representation of the input elements into several representation sub-spaces, the MHSA mechanism allows the neural

network to capture diverse aspects of the input elements simultaneously, leading to better representation learning compared to the single-head self-attention (SHSA) mechanism. The SEG sub-layer ensures the non-linear representation capability of the attention-based sub-element generation layer and generates sub-elements for each input element, and the RC and LN operations stabilize the neural network training. Specifically, $\tilde{\mathbf{X}}$ is first projected to query, key, and value matrices, i.e., $\mathbf{Q} \in \mathbb{R}^{N_I \times d_R}$, $\mathbf{K} \in \mathbb{R}^{N_I \times d_R}$, and $\mathbf{V} \in \mathbb{R}^{N_I \times d_R}$, and then these three matrices are split into N_h sub-matrices, respectively. For the i -th ($i = 1, 2, \dots, N_h$) sub-matrix set, i.e., $\{\mathbf{Q}_i \in \mathbb{R}^{N_I \times d_Q}, \mathbf{K}_i \in \mathbb{R}^{N_I \times d_K}, \mathbf{V}_i \in \mathbb{R}^{N_I \times d_V}\}$, with $d_Q = d_K = d_V = d_R/N_h$, a self-attention score matrix $\mathbf{Z}_i \in \mathbb{R}^{N_I \times N_I}$ is obtained via the scaled dot-product attention (SDPA) [26] as

$$\mathbf{Z}_i = \text{Drop} \left(\frac{\exp(\frac{\mathbf{Q}_i \mathbf{K}_i^T}{\sqrt{d_K}})}{\sum_{j=1}^{N_I} \exp(\frac{\mathbf{Q}_i \mathbf{K}_j^T}{\sqrt{d_K}})}; p_1 \right), \quad (16)$$

where $\text{Drop}(\cdot; p)$ denotes the dropout function with a dropout probability p [27], and the attention-weighted output of the i -th head, denoted by $\mathbf{O}_i \in \mathbb{R}^{N_I \times d_V}$, is obtained as

$$\mathbf{O}_i = \mathbf{Z}_i \mathbf{V}_i. \quad (17)$$

Finally, the attention-weighted outputs of all N_h heads are concatenated and projected to form the output of the MHSA sub-layer, i.e., $\mathbf{X}^{MHSA} \in \mathbb{R}^{N_I \times d_R}$, as

$$\mathbf{X}^{MHSA} = [\mathbf{O}_1, \mathbf{O}_2, \dots, \mathbf{O}_{N_h}] \mathbf{W}^O, \quad (18)$$

where $\mathbf{W}^O \in \mathbb{R}^{d_R \times d_R}$ is a learnable weight matrix. The outputs of the RC and LN operations around the MHSA sub-layer, denoted by $\mathbf{X}^{RC1} \in \mathbb{R}^{N_I \times d_R}$ and $\mathbf{X}^{LN1} \in \mathbb{R}^{N_I \times d_R}$, respectively, can be formulated by

$$\mathbf{X}^{RC1} = \mathbf{X}^{MHSA} + \tilde{\mathbf{X}}, \quad (19)$$

and

$$\mathbf{X}^{LN1} = \frac{\mathbf{X}^{RC1} - \mu_{\mathbf{X}^{RC1}}}{\sigma_{\mathbf{X}^{RC1}}} \odot \mathbf{g}^{LN1} + \mathbf{b}^{LN1}, \quad (20)$$

$$\mu_{\mathbf{X}^{RC1}} = \frac{1}{d_R} \sum_{i=1}^{d_R} \mathbf{X}_{:,i}^{RC1}, \quad (21)$$

$$\sigma_{\mathbf{X}^{RC1}} = \sqrt{\frac{1}{d_R} \sum_{i=1}^{d_R} (\mathbf{X}_{:,i}^{RC1} - \mu_{\mathbf{X}^{RC1}})^2}, \quad (22)$$

where $\mu_{\mathbf{X}^{RC1}} \in \mathbb{R}^{N_I \times 1}$ and $\sigma_{\mathbf{X}^{RC1}} \in \mathbb{R}^{N_I \times 1}$ denote the mean and standard deviation of \mathbf{X}^{RC1} , $\mathbf{g}^{LN1} \in \mathbb{R}^{1 \times d_R}$ and $\mathbf{b}^{LN1} \in \mathbb{R}^{1 \times d_R}$ are learnable affine transformation parameters, and \odot is the Hadamard product. The output of the SEG sub-layer, i.e., $\mathbf{X}^G \in \mathbb{R}^{N_I \times (r \times d_R)}$, can be formulated by

$$\mathbf{X}^G = (\text{Drop}(\text{ReLU}(\mathbf{X}^{RC1} \mathbf{W}^{G1} + \mathbf{b}^{G1}); p_2)) \mathbf{W}^{G2} + \mathbf{b}^{G2}, \quad (23)$$

where p_2 is a dropout probability, $\text{ReLU}(\cdot)$ is the rectified linear unit (ReLU) activation function, $\mathbf{W}^{G1} \in \mathbb{R}^{d_R \times d_G}$ and $\mathbf{W}^{G2} \in \mathbb{R}^{d_G \times (r \times d_R)}$ are learnable weight matrices where $d_G = d_R$, and $\mathbf{b}^{G1} \in \mathbb{R}^{1 \times d_G}$ and $\mathbf{b}^{G2} \in \mathbb{R}^{1 \times (r \times d_R)}$ are learnable bias vectors. r is the number of sub-elements to be generated, which is also known as the upscale factor. The output of the RC operation around the SEG sub-layer, i.e., $\mathbf{X}^{RC2} \in \mathbb{R}^{N_I \times (r \times d_R)}$, can be formulated by

$$\mathbf{X}^{RC2} = \mathbf{X}^G + \mathbf{X}^{LN1} \mathbf{W}^{RC2}, \quad (24)$$

where $\mathbf{W}^{RC2} \in \mathbb{R}^{d_R \times (r \times d_R)}$ is a learnable weight matrix. The output of the LN operation around the SEG sub-layer, i.e., $\mathbf{X}^{LN2} \in \mathbb{R}^{N_I \times (r \times d_R)}$, can be formulated by

$$\mathbf{X}^{LN2} = \frac{\mathbf{X}^{RC2} - \mu_{\mathbf{X}^{RC2}}}{\sigma_{\mathbf{X}^{RC2}}} \odot \mathbf{g}^{LN2} + \mathbf{b}^{LN2}, \quad (25)$$

$$\mu_{\mathbf{X}^{RC2}} = \frac{1}{d_R} \sum_{i=1}^{d_R} \mathbf{X}_{:,i}^{RC2}, \quad (26)$$

$$\sigma_{\mathbf{X}^{RC2}} = \sqrt{\frac{1}{d_R} \sum_{i=1}^{d_R} (\mathbf{X}_{:,i}^{RC2} - \mu_{\mathbf{X}^{RC2}})^2}, \quad (27)$$

where $\mu_{\mathbf{X}^{RC2}} \in \mathbb{R}^{N_I \times 1}$ and $\sigma_{\mathbf{X}^{RC2}} \in \mathbb{R}^{N_I \times 1}$ denote the mean and standard deviation of \mathbf{X}^{RC2} , $\mathbf{g}^{LN2} \in \mathbb{R}^{1 \times (r \times d_R)}$ and $\mathbf{b}^{LN2} \in \mathbb{R}^{1 \times (r \times d_R)}$ are learnable affine transformation parameters.

After the attention-based sub-element generation layer generates r sub-elements for each input element, the sub-element shuffle layer shuffles these sub-elements together to form a new input element matrix as

$$\mathbf{X}^E = [\mathbf{R}(\mathbf{X}_{:,1:r}^{LN2}), \mathbf{R}(\mathbf{X}_{:,r+1:2r}^{LN2}), \dots, \mathbf{R}(\mathbf{X}_{:,r \times d_R - r + 1:r \times d_R}^{LN2})], \quad (28)$$

where $\mathbf{X}^E \in \mathbb{R}^{(r \times N_I) \times d_R}$, and \mathbf{R} denotes a rearrange operator that transforms the size of $\mathbf{X}_{:,i:i+r-1}^{LN2} \in \mathbb{R}^{N_I \times r}$ into $(r \times N_I) \times 1$. Therefore, through the ASEEM, the original input $\mathbf{X} \in \mathbb{R}^{N_I \times d_R}$ can be extrapolated to $\mathbf{X}^E \in \mathbb{R}^{(r \times N_I) \times d_R}$ effectively via to sub-element generation.

2) *Progressive Extrapolation Architecture*: Since directly extrapolating partial CSI to full CSI is significantly challenging, especially when the spatial and frequency compression ratios are large, we propose to conduct spatial and frequency channel extrapolation progressively with the progressive extrapolation architecture. The spatial extrapolation and frequency extrapolation are organized in a sequential manner, i.e., the N_{SE} spatial ASEEMs of the progressive spatial extrapolation block first progressively extrapolate partial spatial CSI to full spatial CSI, and then the N_{FE} frequency ASEEMs of the progressive frequency extrapolation block progressively extrapolate partial frequency CSI to full frequency CSI. During this process, the sizes of the inputs to the i -th spatial ASEEM, i.e., $\mathbf{X}^S(i)$, and the j -th frequency ASEEM, i.e., $\mathbf{X}^F(j)$, progressively increase as

$$\mathbf{X}^S(i) \in \mathbb{R}^{(r_s^{i-1} \times N_{SI}) \times d_{SR}}, \quad i = 1, 2, \dots, N_{SE}, \quad (29)$$

$$\mathbf{X}^F(j) \in \mathbb{R}^{(r_f^{j-1} \times N_{FI}) \times d_{FR}}, \quad j = 1, 2, \dots, N_{FE}, \quad (30)$$

where r_s , N_{SI} , and d_{SR} are the spatial upscale factor, the number of initial spatial input elements, and the spatial representation dimension, respectively; and r_f , N_{FI} , and d_{FR} are the frequency upscale factor, the number of initial frequency input elements, and the frequency representation dimension, respectively. And N_{SE} and N_{FE} are determined by

$$N_{SE} = \lceil \log_{r_f}^{R_s} \rceil, \quad (31)$$

$$N_{FE} = \lceil \log_{r_f}^{R_f} \rceil, \quad (32)$$

where $\lceil \cdot \rceil$ denotes the ceiling function. Correspondingly, the sizes of the outputs of the i -th spatial ASEEM, i.e., $\mathbf{X}^{SE}(i)$, and the j -th frequency ASEEM, i.e., $\mathbf{X}^{FE}(j)$, progressively increase as

$$\mathbf{X}^{SE}(i) \in \mathbb{R}^{(r_s^i \times N_{SI}) \times d_{SR}}, \quad i = 1, 2, \dots, N_{SE}, \quad (33)$$

$$\mathbf{X}^{FE}(j) \in \mathbb{R}^{(r_f^j \times N_{FI}) \times d_{FR}}, \quad j = 1, 2, \dots, N_{FE}. \quad (34)$$

In addition, the sizes of the spatial positional encoding (SPE) for the i -th spatial ASEEM and the frequency positional encoding (FPE) for the j -th frequency ASEEM progressively increase as

$$\mathbf{P}^S(i) \in \mathbb{R}^{(r_s^{i-1} \times N_{SI}) \times d_{SR}}, \quad i = 1, 2, \dots, N_{SE}, \quad (35)$$

$$\mathbf{P}^F(j) \in \mathbb{R}^{(r_f^{j-1} \times N_{FI}) \times d_{FR}}, \quad j = 1, 2, \dots, N_{FE}. \quad (36)$$

C. Model Training

The proposed KDD-SFCEN is trained via the mean squared error (MSE) loss defined as⁵

$$L_1 = \mathbb{E}_{N_{train}} (\|\mathbf{H}\{s, 0\} - F_{ssucc}(\mathbf{Y}^p\{s, 0\}, \mathbf{S}^p\{s, 0\})\|_2^2), \quad (37)$$

where $\mathbb{E}_{N_{train}}(\cdot)$ denotes the expectation over N_{train} training samples, and $\|\cdot\|_2$ denotes the L2 norm.

After obtaining the estimated uplink channel, the slot-level channel extrapolation can then be conducted to enlarge the pilot signal period T_p and further reduce the overall pilot training overhead C_o .

IV. CHANNEL RECIPROCITY AND TEMPORAL DEPENDENCY AIDED SLOT-LEVEL CHANNEL EXTRAPOLATION

An accurate initial state is essential to the subsequent extrapolations in the temporal domain. Thanks to the uplink-downlink channel reciprocity in TDD systems, the downlink channel of the first downlink slot of a sub-frame can be accurately derived from the uplink channel of the sub-frame's special slot via uplink-downlink channel calibration. The derived downlink channel provides an accurate initial state for predicting downlink channels at future downlink slots. Recent advances in generative AI, e.g., the ChatGPT [28], have witnessed the superiority of autoregressive generative models, specifically generative Transformers [20], for processing sequential data. For time-varying channels, which are also one kind of sequential data, generative Transformers are also promising on account of their capabilities in learning complicated temporal dependencies and autoregressive modeling. Therefore, in this section, we propose the TUDCEN consisting of the UDCCN and the DCEN to achieve slot-level channel extrapolation. The architecture of the TUDCEN is shown in Fig. 2. Specifically, the UDCCN realizes uplink-downlink channel calibration for initialization by exploiting the uplink-downlink channel reciprocity, and the DCEN mainly exploits the proposed spatial-frequency sampling embedding module to reduce the computational complexity and generative Transformers for temporal dependency learning and autoregressive downlink channel extrapolation.

A. Channel Reciprocity Aided Uplink-Downlink Channel Calibration

Although the physical uplink-downlink channels within the channel coherence time are generally reciprocal, uplink-downlink channel calibration is practically necessary to compensate for the hardware asymmetry in transceivers [22]. The uplink-downlink channel extrapolation can be formulated by

$$\hat{\mathbf{H}}^d\{s, 1\} = F_{udcc}(\hat{\mathbf{H}}\{s, 0\}), \quad (38)$$

where F_{udcc} denotes the UDCCN.

To calibrate the downlink channel from the estimated uplink channel, both the spatial and frequency characteristics of

the channels should be exploited. Therefore, we propose the two-dimensional (2D) convolution-based calibration network for uplink-downlink channel calibration. The 2D convolution operation can capture spatial and frequency characteristics for accurate calibration. In addition, the ReLU activation function and the RC operation are also applied to improve the network's non-linear representation capability and stabilize the network training, respectively. The input to the UDCCN is obtained by

$$\underline{\mathbf{X}}^U = f_{C \rightarrow \mathbb{R}}(\hat{\mathbf{H}}\{s, 0\}), \quad (39)$$

where $\underline{\mathbf{X}}^U \in \mathbb{R}^{(N_T \times N_R) \times N_c \times 2}$ is a real-valued tensor form representation of the estimated uplink channel and the 2 in the dimensions comes from the concatenated real and imaginary parts of the original complex-valued matrix, and $f_{C \rightarrow \mathbb{R}}$ is a function to transform the original complex-valued matrix form representation to the real-valued tensor form representation. The output of the UDCCN, denoted by $\underline{\mathbf{X}}^D \in \mathbb{R}^{(N_T \times N_R) \times N_c \times 2}$, can be formulated by

$$\tilde{\underline{\mathbf{X}}}^D = \text{ReLU}(\text{Conv}^{k \times k}(\underline{\mathbf{X}}^U); \mathbf{W}^{Conv}) + \underline{\mathbf{X}}^U, \quad (40)$$

$$\underline{\mathbf{X}}^D = \tilde{\underline{\mathbf{X}}}^D \mathbf{W}^D \quad (41)$$

where $\text{Conv}^{k \times k}$ is a 2D convolution operation with kernel size being $k \times k$ and parameterized by $\mathbf{W}^{Conv} \in \mathbb{R}^{(2k^2) \times d_f}$, d_f is the feature dimension, $\tilde{\underline{\mathbf{X}}}^D \in \mathbb{R}^{(N_T \times N_R) \times N_c \times (2+d_f)}$ is the intermediate feature representation, and $\mathbf{W}^D \in \mathbb{R}^{(2+d_f) \times 2}$ is a learnable weight matrix that projects the intermediate feature representation to the final output $\underline{\mathbf{X}}^D$. Then, the calibrated downlink channel can be obtained by

$$\hat{\mathbf{H}}^d\{s, 1\} = f_{\mathbb{R} \rightarrow C}(\underline{\mathbf{X}}^D), \quad (42)$$

where $f_{\mathbb{R} \rightarrow C}$ is a function to transform the real-valued tensor form representation to the original complex-valued matrix form representation.

B. Temporal Dependency Learning and Downlink Channel Extrapolation

It is worth mentioning that the downlink channel extrapolation problem is conducted along the time domain and aims to predict channels at future slots, which can be regarded as a time series prediction problem. However, different from general time series prediction problems, historical observations in the investigated downlink channel extrapolation problem (i.e., downlink channels at all downlink slots) can not be obtained unless huge time-frequency resources were spent to conduct channel estimation for all downlink slots. As a result, the performance of widely adopted sequence-to-sequence (Seq2Seq) prediction schemes in related works [18] would be significantly degraded due to the lack of available historical channel information. Note that like many real-world phenomena, wireless channels exhibit temporal dependencies over time. Then, based on the chain rule in the probability theory, the joint probability of the concatenated downlink channels can be expressed as

$$\begin{aligned} & P([\hat{\mathbf{H}}^d\{s, 1\}, \hat{\mathbf{H}}^d\{s, 2\}, \dots, \hat{\mathbf{H}}^d\{s, N_{slot} - 1\}]) = \\ & P(\hat{\mathbf{H}}^d\{s, 1\}) \times P(\hat{\mathbf{H}}^d\{s, 2\} | \hat{\mathbf{H}}^d\{s, 1\}) \times \dots \times \\ & P(\hat{\mathbf{H}}^d\{s, N_{slot} - 1\} | \hat{\mathbf{H}}^d\{s, 1\} \hat{\mathbf{H}}^d\{s, 2\} \hat{\mathbf{H}}^d\{s, N_{slot} - 2\}). \end{aligned} \quad (43)$$

Inspired by this, the objective of the downlink channel extrapolation is

$$\begin{aligned} & \hat{\mathbf{H}}^d\{s, t\} = F_{dce}([\hat{\mathbf{H}}^d\{s, 1\}, \dots, \hat{\mathbf{H}}^d\{s, t-1\}]), \\ & \text{for } t = 2, 3, \dots, N_{slot} - 1, \end{aligned} \quad (44)$$

⁵The inputs to F_{ssucc} are actually real-valued tensors transformed from $\mathbf{Y}^p\{s, 0\}$ and $\mathbf{S}^p\{s, 0\}$. We use their original complex-valued matrix form in the loss expression for simplicity.

where F_{dce} denotes the DCEN, such that (43) can be achieved and the downlink channels from the 2nd slot to the $(N_{slot} - 1)$ -th slot can be extrapolated given only $\hat{\mathbf{H}}^d\{s, 1\}$. It is worth noting that (44) actually refers to the autoregressive generation manner and the DCEN should thus be an autoregressive model. And considering that $\hat{\mathbf{H}}^d\{s, t\}$, $t = 1, 2, \dots, N_{slot} - 1$ are dependent, capturing these temporal dependencies among them would be beneficial to achieve (44). To this end, we propose the DCEN constituted by (inverse) spatial-frequency patch embedding layers and generative Transformers for temporal dependency learning and autoregressive downlink channel extrapolation. The architecture of the DCEN is also shown in Fig. 2.

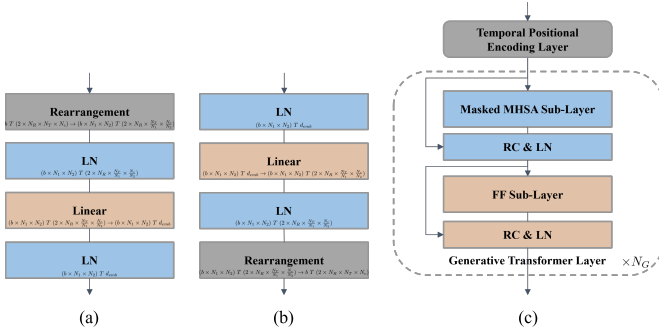


Fig. 4. The architecture of the (inverse) spatial-frequency sampling embedding layers and the generative Transformer.

1) *Spatial-Frequency Sampling Embedding*: Due to the large number of antennas and subcarriers, the downlink channels' spatial and frequency domain representation must be compressed to reduce the computational complexity of downlink channel extrapolation. Therefore, we propose the spatial-frequency sampling embedding layer. The spatial-frequency sampling embedding layer consists of one rearrangement operation, two LN operations, and one linear layer, as Fig. 4 (a) shows. The rearrangement operation splits the N_T transmit antennas and N_c subcarriers into N_1 transmit antenna groups and N_2 subcarrier groups, respectively. Each transmit antenna group has $\frac{N_T}{N_1}$ antennas and each subcarrier group has $\frac{N_c}{N_2}$ subcarriers. Note that since the number of UE antennas, i.e., N_R , is generally small, it is not necessary to further split UE antennas. Specifically, the rearrangement operation rearranges the sample dimension (known as the batch size N_b), N_1 , and N_2 together to form a new sample dimension, and consequently reforms a representation dimension of length $2 \times N_R \times \frac{N_T}{N_1} \times \frac{N_c}{N_2}$. Then, the dimension of the reformed representation is normalized by the first LN operation. Following that, the dimension is further projected to an embedding dimension d_{emb} by the linear layer and normalized by the second LN operation. Straightforwardly, the spatial-frequency sampling embedding layer samples the spatial and frequency domain representation of downlink channels with a spatial sampling factor N_1 and a frequency sampling factor N_2 to reduce the representation dimension by resorting to the spatial and frequency correlations of downlink channels. Meanwhile, the N_1 sampled transmit antenna groups and N_2 sampled subcarrier groups are combined to facilitate model training. It is worth noting that after the generative Transformers, the inverse spatial-frequency sampling embedding layer is applied to transform the sampled representation dimension back to the original spatial and frequency domain representation. In the inverse spatial-frequency sampling embedding layer, all layers and operations are placed and operated in the inverse direction

to the spatial-frequency sampling embedding layer, as Fig. 4 (b) shows.

2) *Generative Transformer and Masked MHSA Mechanism*: The generative Transformer is one kind of autoregressive generative models that was proposed for text generation and is known as one of the most important driven forces for the transformative ChatGPT. The core of the generative Transformer is the masked MHSA mechanism, a pivotal component enabling the effective processing of input sequences. The masked MHSA mechanism allows the model to capture long-term dependencies among elements of input sequences and selectively attend to these elements while preventing it from looking ahead during training by masking future elements. To learn temporal dependencies efficiently for downlink channel extrapolation, we propose the generative Transformer-based downlink channel extrapolation network. The architecture shown in Fig. 4 (c) depicts that the proposed generative Transformer consists of a temporal positional encoding layer and N_G generative Transformer layers. The temporal positional encoding layer is similar to (13) - (14). Each generative Transformer layer further consists of a masked MHSA sub-layer, a feed-forward (FF) sub-layer, and also RC and LN operations around each of the two sub-layers. Compared with the MHSA sub-layer, a masking operation is introduced before the query, key, and value projections in the masked MHSA sub-layer. The output of the masking operation, denoted by $\tilde{\mathbf{X}}^M \in \mathbb{R}^{N_I' \times d_R}$ with N_I' being the number of input elements and d_R being the representation dimension of each input element, can be expressed by

$$\tilde{\mathbf{X}}^M = \tilde{\mathbf{X}}' + \mathbf{M}, \quad (45)$$

where $\tilde{\mathbf{X}}' \in \mathbb{R}^{N_I' \times d_R}$ is the input matrix to the masked MHSA sub-layer, and $\mathbf{M} \in \mathbb{R}^{N_I' \times d_R}$ is a lower-triangular masking matrix whose lower triangular elements are all negative infinity. Note that the masked MHSA sub-layer is with N_h' attention heads and a dropout probability p_3 . The FF sub-layer can be formulated by

$$\mathbf{X}^{FF} = (\text{Drop}(\text{ReLU}(\mathbf{X}^{RC1} \mathbf{W}^{FF1} + \mathbf{b}^{FF1}); p_4)) \mathbf{W}^{FF2} + \mathbf{b}^{FF2}, \quad (46)$$

where $\mathbf{X}^{FF} \in \mathbb{R}^{N_I' \times d_R}$, p_4 is a dropout probability, $\mathbf{W}^{FF1} \in \mathbb{R}^{d_R \times d_{FF}}$ and $\mathbf{W}^{FF2} \in \mathbb{R}^{d_{FF} \times d_R}$ are learnable weight matrices, and $\mathbf{b}^{FF1} \in \mathbb{R}^{1 \times d_{FF}}$ and $\mathbf{b}^{FF2} \in \mathbb{R}^{1 \times d_R}$ are learnable bias vectors. The two sets of RC and LN operations around the masked MHSA sub-layer and the FF sub-layer are organized and computed similarly to the two sets of RC and LN operations shown in (19) to (22) and (24) to (27), respectively.

C. Computational Complexity Analysis

Here we analyze the computational complexity of the spatial-frequency sampling embedding layer, and compare it with the most common existing spatial-frequency domain representation extractors for high-dimensional inputs: 1) the 2D convolution layer and 2) the fully-connected layer.

The time complexity of the spatial-frequency sampling embedding layer can be calculated as

$$\mathcal{O}(\text{SFSE}) = \mathcal{O}(2N_R N_T N_c d_R'), \quad (47)$$

and the space complexity (i.e., the number of learnable parameters) can be calculated as

$$N_\theta(\text{SFSE}) = \mathcal{O}(2N_R \frac{N_T}{N_1} \frac{N_c}{N_2} d_R'). \quad (48)$$

The 2D convolution layer is blamed for high time complexity and the fully-connected layer is blamed for high space

complexity when dealing with high-dimensional inputs. The time complexity of the 2D convolution layer can be calculated as

$$\mathcal{O}(2\text{D Conv}) = \mathcal{O}(2k^2 N_R N_T N_c d'_R), \quad (49)$$

where $k \geq 1$ is the convolution kernel size. It is worth emphasizing that to reduce the spatial and frequency dimensions of the input, the stride of the 2D convolution layer should be set larger than 1, or a pooling layer should be applied after the 2D convolution layer. Generally, it requires a deep convolutional network consisting of many 2D convolution layers to gradually reduce the spatial and frequency dimensions of the input. This thus further increases the time complexity of using 2D convolution layers for obtaining the spatial-frequency domain representation for high-dimensional CSI matrices. While for the spatial-frequency sampling embedding layer, one layer is enough to obtain the spatial-frequency domain representation for high-dimensional CSI matrices. Therefore, the spatial-frequency sampling embedding layer is $\gg k^2$ times more efficient than the deep convolutional network.

The fully-connected layer has the same time complexity as the spatial-frequency sampling embedding layer. However, the space complexity of the fully-connected layer is huge, which can be calculated as

$$N_\theta(\text{FC}) = \mathcal{O}(2N_R N_T N_c d'_R), \quad (50)$$

which is $N_1 \times N_2$ times as the spatial-frequency sampling embedding layer, leading to prohibitive memory usage and a challenging optimization process when training the neural network.

D. Model Training

To train the model efficiently, the sliding window method is applied to generate windowed temporal channel slices. The window length is $l_w = N_{slot}$ and the sliding stride is $l_s = N_{slot}$. Denoting the number of training samples and the number of sub-frames as N_{train} and N_{sf} , respectively, the normalized mean squared error (NMSE) loss function for training the UDCCN is defined as

$$L_2 = \mathbb{E}_{N_w} \left\{ \frac{\|\mathbf{H}^d\{s, 1\} - F_{udcc}(\hat{\mathbf{H}}\{s, 0\})\|_2^2}{\|\mathbf{H}^d\{s, 1\}\|_2^2} \right\}, \quad (51)$$

where $N_w = N_{train} * N_{sf}$ is the number of slices generated from all training samples. The NMSE loss function for training the DCEN is defined as

$$L_3 = \mathbb{E}_{N_w} \left\{ \frac{\sum_{t=2}^{N_{slot}-1} \|\mathbf{H}^d\{s, t\} - F_{dce}(\hat{\mathbf{H}}^d\{s, 1\})\|_2^2}{N_{slot} - 2} \right\}. \quad (52)$$

V. SIMULATIONS

In this section, we first introduce the simulation setup for numerical evaluations. Then, we compare the proposed KDD-SFCEN with traditional and DNN-based extrapolation methods under various spatial and frequency compression ratios, SNRs, and UE velocity settings. We then compare the TUDCEN with DNN-based temporal channel extrapolators. Finally, we present and analyze the overall performance of the proposed framework in terms of the achievable sum-rate of the system.

A. Simulation Setup

1) *Simulation Dataset and Parameters*: The simulation dataset is constructed using the MATLAB 5G toolbox [29]. We consider a mmWave massive MIMO system with one BS and one single user. Uniform linear arrays (ULAs) are

employed at the BS and the UE with $N_T = 32$ and $N_R = 4$. The system works in the TDD mode and operates with the OFDM modulation. The system comprises 52 RBs, and each RB is formed by 12 subcarriers and 14 OFDM symbols according to the 5G specification [21]. In addition, the system follows the 5G frame structure shown in Fig. 1 (e) with $\mu = 3$ and $N_{slot} = 8$, and note that the SRS period $T_p = 1$ ms (i.e., once per sub-frame). The SRS is configured at the last symbol index of each special slot. We adopt the clustered delay line (CDL)-B MIMO channel model to generate channel instances [30] at various UE mobility settings. 95 channel instances are generated for constructing training and validation samples, and the BS transmits the SRS to the UE via these channel instances at the special slot of each sub-frame in 10 frames (i.e., in total 100 sub-frames / 800 slots) at a signal-to-noise ratio (SNR) level of 5 dB (i.e., $\gamma_{SNR} = 5$ dB) and the UE mobility of 60 km/h (i.e., $v = 60$ km/h). 5 channel instances are generated for constructing testing samples, and the BS transmits the SRS to the UE via these channel instances at the special slots of 100 sub-frames at different SNR levels. The SRS pattern is configured based on the spatial compression ratio R_s and the frequency compression level R_f as depicted in Section II-C. As a result, for a given (R_s, R_f) pair, 9,500 samples are generated for training (9,000 samples) and validation (500 samples); for a given $(R_s, R_f, \gamma_{SNR}, v)$ pair, 500 samples are generated for testing. The spatial compression ratios, frequency compression ratios, SNR levels, UE mobility, and other key system parameters are listed in Table I. The hyper-parameter settings of the proposed KDD-SFCEN and the TUDCEN are shown in Table II and Table III, respectively.

TABLE I
SYSTEM PARAMETER SETTINGS.

Parameter	Value
Channel model	CDL-B
Carrier frequency	28 GHz
SRS period T_p	1 ms
Subcarrier spacing	120 kHz
The number of frames	10
Numerology μ	3
The number of slots per sub-frame N_{slot}	8
The number of sub-frames N_{sf}	100
The number of BS antennas N_T	32
The number of UE antennas N_R	4
The number of subcarriers N_c	624
Spatial compression ratio R_s	1, 2, 4, 8
Frequency compression ratio R_f	2, 4, 8, 16
SNR γ_{SNR} (dB)	-5, 0, 5 (training), 10, 15, 20
UE velocity v (km/h)	5, 15, 30, 60 (training), 90, 120
The number of training N_{train}	9,000
The number of validation samples N_{valid}	500
The number of testing samples N_{test}	500

TABLE II
HYPER-PARAMETER SETTINGS FOR THE KDD-SFCEN.

Hyper-parameter	Setting
Representation dimension in the KDD-SFCEN d_R	512
No. of attention head N_h	4
MHSA sub-layer dropout probability p_1	0.5
SEG sub-layer dropout probability p_2	0.5
Batch size	64
Initial learning rate	$6e - 5$

2) *Evaluation Metrics*: For uplink channel estimation, uplink-downlink channel calibration, and also downlink channel extrapolation, the NMSE in dB is adopted to evaluate the channel estimation performance, which is defined as

$$\text{NMSE}\{t\} = 10 * \log \left(\frac{\sum_{j=1}^{N_{test}} \sum_{s=1}^{N_{sf}} \frac{\|\bar{\mathbf{H}}^j\{s, t\} - \hat{\bar{\mathbf{H}}}^j\{s, t\}\|_2^2}{\|\bar{\mathbf{H}}^j\{s, t\}\|_2^2}}{N_{test} N_{sf}} \right), \quad (53)$$

TABLE III
HYPER-PARAMETER SETTINGS FOR THE TUDCEN.

Hyper-parameter	Setting
Calibration feature dimension d_f	32
Convolution kernel size k	3
Embedding dimension d_{emb}	512
Spatial sampling factor N_1	4
Frequency sampling factor N_2	12
Representation dimension in the TUDCEN d'_R	512
No. of attention head N'_h	4
MHSA sub-layer dropout probability p_3	0.5
FF sub-layer dropout probability p_4	0.5
No. of generative Transformer layers	4
Batch size N_b	100
Initial learning rate	$6e-5$

where N_{test} is the number of testing samples. Specifically, for uplink channel estimation, $\bar{\mathbf{H}}$ refers to \mathbf{H} and $t = 0$; for uplink-downlink channel calibration, $\bar{\mathbf{H}}$ refers to \mathbf{H}^d and $t = 1$; for downlink channel extrapolation, $\bar{\mathbf{H}}$ refers to \mathbf{H}^d , and $t = 2, 3, \dots, N_{slot} - 1$.

In addition, the achievable sum-rate in bps/Hz is adopted to evaluate the system performance, which is defined as

$$R\{t\} = \sum_{j=1}^{N_{test}} \sum_{s=1}^{N_{sf}} \log_2 \left(1 + \frac{\mathbf{H}^d\{s,t\}\mathbf{F}\{s,t\}(\mathbf{H}^d\{s,t\}\mathbf{F}\{s,t\})^H}{N_R\sigma_n^2} \right), \quad (54)$$

where σ_n^2 is the noise power.

B. Performance Evaluation of Proposed KDD-SFCEN

We first compare the performance of the proposed KDD-SFCEN and traditional and DNN-based extrapolation methods for frequency domain channel extrapolation, including the linear spline interpolation method [9], the DFT-interpolation method [9], and the SRCNN-based method [10]. It can be seen from Fig. 5 that the proposed KDD-SFCEN outperforms all baselines at the same R_f . In addition, the proposed KDD-SFCEN can achieve a better NMSE performance at $R_f = 16$ than traditional baselines at $R_f = 2$, which indicates that the proposed KDD-SFCEN can reduce the pilot training overhead up to 8 times from the frequency domain perspective compared with traditional baselines. Similarly, the proposed KDD-SFCEN can reduce the pilot training overhead up to 4 times from the frequency domain perspective compared with the SRCNN-based method.

We then compare the proposed KDD-SFCEN with traditional and DNN-based extrapolation methods for spatial domain channel extrapolation, including the linear spline interpolation method [9], the DFT-interpolation method [9], and the FCNN-based method [13]. As shown in Fig. 6, the proposed KDD-SFCEN achieves better NMSE performance than all these baselines at the same R_s . Moreover, the proposed KDD-SFCEN at $R_s = 8$ surpasses the FCNN-based method and achieves a similar NMSE performance as traditional baselines at $R_s = 1$, indicating that the proposed KDD-SFCEN can reduce the pilot training overhead around 8 times from the spatial domain perspective compared with existing baselines.

It can be seen from Fig. 5 and Fig. 6 that when $R_f = 8$ or $R_s = 4$ (corresponding to a 4-fold reduction in pilot training overhead compared to $R_f = 2$ or $R_s = 1$), the NMSE performance of uplink channel estimation with the proposed KDD-SFCEN is around -9 dB and -10 dB, respectively, which is already good enough for uplink channel estimation. However, since the downlink CSI at future slots has to be extrapolated based on the estimated uplink CSI, it would be better to improve the performance of uplink channel

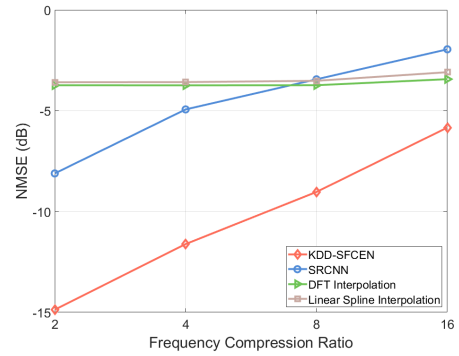


Fig. 5. The NMSE performance of uplink channel estimation versus the frequency compression ratio R_f at $R_s = 1$, $v = 60$ km/h, and $\gamma_{SNR} = 20$ dB.

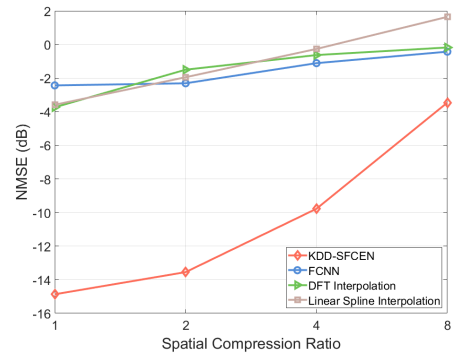


Fig. 6. The NMSE performance of uplink channel estimation versus the spatial compression ratio R_s at $R_f = 2$, $v = 60$ km/h, and $\gamma_{SNR} = 20$ dB.

estimation as much as possible. From Fig. 5 and Fig. 6, increasing R_f from 2 to 4 or increasing R_s from 1 to 2 leads to a minimum performance degradation compared to other increasing cases in R_f or R_s .⁶ These actually reflect the marginal effects of pilots in either the frequency domain or the spatial domain. Therefore, it is promising that we combine $R_f = 4$ and $R_s = 2$ for joint spatial and frequency domain channel extrapolation to improve the uplink channel estimation performance and restrict the performance degradation due to the reduction of pilot symbols in the frequency domain and the spatial domain. Fig. 7 shows the NMSE performance of uplink channel estimation versus γ_{SNR} at $R_f = 4$ and $R_s = 2$ (solid lines), where we further compare the proposed KDD-SFCEN with the SF-CNN [19] in addition to the linear spline interpolation method [9] and the DFT-interpolation method [9]. The simulation results show that the NMSE performance of the KDD-SFCEN reaches near -12 dB at $\gamma_{SNR} = 20$ dB and the KDD-SFCEN outperforms the SF-CNN about 4 dB and the traditional baselines about 9 dB at $\gamma_{SNR} \geq 0$ dB. Even with a low SNR, i.e., $\gamma_{SNR} = -5$ dB, the KDD-SFCEN can achieve a performance enhancement around 3.5 dB and 5 dB compared with the SF-CNN and traditional baselines. Moreover, the NMSE performance of the linear spline interpolation method, the DFT-interpolation method, and SF-CNN at $R_f = 2$ and $R_s = 1$ are also shown in Fig. 7 with dotted lines, indicating that the KDD-SFCEN can reduce the pilot training overhead up to 4 times compared to existing methods. These results demonstrate that combining spatial and frequency domain channel extrapolation can further improve the channel estimation performance (2 dB to

⁶Note that from Fig. 5 that increasing R_f leads to a near linear NMSE (in dB) performance degradation, thus the actual performance degradation increases in this progress.

3 dB) with the same pilot training overhead (i.e., a 4-fold reduction in pilot training overhead).

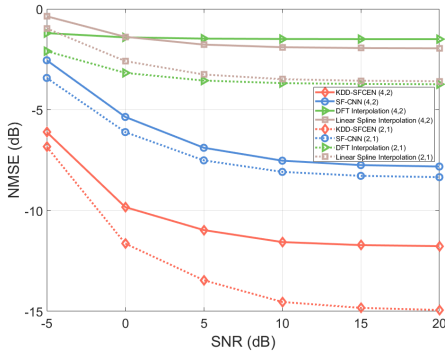


Fig. 7. The NMSE performance of uplink channel estimation versus the SNR γ_{SNR} at $v = 60$ km/h, with $(R_f = 4, R_s = 2)$ or $(R_f = 2, R_s = 1)$.

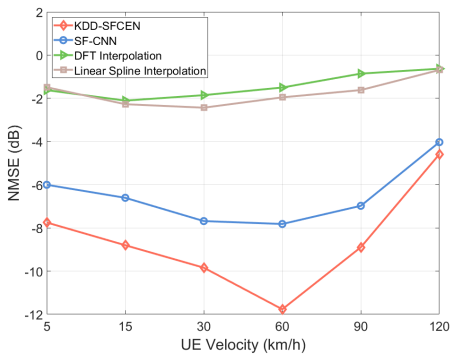


Fig. 8. The NMSE performance of uplink channel estimation versus the UE velocity v at $R_f = 4, R_s = 2$, and $\gamma_{SNR} = 20$ dB.

We further examine the robustness to the UE velocity of the proposed KDD-SFCEN. As depicted in Fig. 8, DNN-based methods (including the proposed KDD-SFCEN and the SF-CNN) achieve the best performance when the testing UE velocity is equal to the training UE velocity (i.e., $v = 60$ km/h), showing their capability in capturing spatial-frequency domain features and improving channel estimation accuracy. When the testing UE velocity decreases or increases, the performance of the DNN-based methods degrades. Moreover, the greater the deviation of the testing UE velocity from the training UE velocity, the more significant the performance degradation will be. Nonetheless, the proposed KDD-SFCEN achieves sufficient channel estimation accuracy (around or above -8 dB) and outperforms all baselines with $v \leq 90$ km/h at $R_f = 4$ and $R_s = 2$, showing its outstanding robustness to the UE velocity.

C. Performance Evaluation of Proposed TUDCEN

Since uplink-downlink channel calibration is simple but necessary, we do not compare the proposed UDCCN with other methods. Instead, we apply the UDCCN to the aforementioned spatial-frequency channel extrapolation methods and present their performance on estimating the channel at the first downlink slot with or without calibration. As shown in Fig. 9, all methods generally benefit from the uplink-downlink channel calibration, demonstrating that uplink-downlink channel calibration is necessary and the proposed UDCCN is simple but effective to conduct uplink-downlink channel calibration.

We then evaluate the performance of slot-level channel extrapolation with the proposed TUDCEN and a baseline

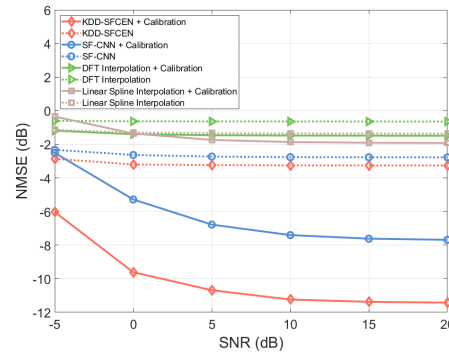


Fig. 9. The NMSE performance of uplink-downlink channel calibration versus the SNR γ_{SNR} at $R_f = 4, R_s = 2$, and $v = 60$ km/h.

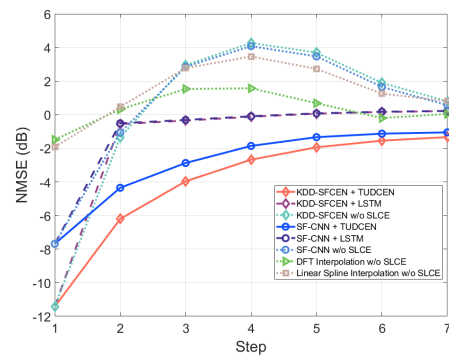


Fig. 10. The NMSE performance of slot-level channel extrapolation versus the index of a slot in a sub-frame at $R_f = 4, R_s = 2, \gamma_{SNR} = 20$ dB, and $v = 60$ km/h.

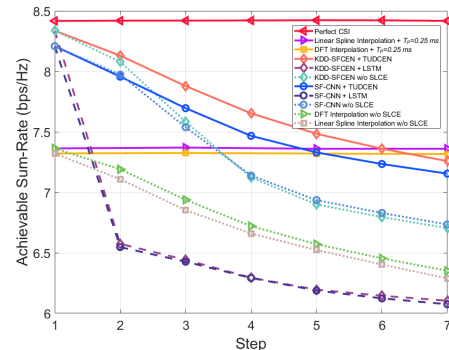


Fig. 11. The achievable sum-rate performance of slot-level channel extrapolation versus the index of a slot in a sub-frame at $R_f = 4, R_s = 2, \gamma_{SNR} = 20$ dB, and $v = 60$ km/h.

temporal channel extrapolation method. i.e., the LSTM-based channel predictor [17]. Note that the uplink-downlink channel calibration is applied to all methods. We further combine the proposed KDD-SFCEN and the baseline uplink channel estimation method SF-CNN with the proposed TUDCEN and the LSTM. The NMSE performance and the achievable sum-rate performance at $R_f = 4, R_s = 2, \gamma_{SNR} = 20$ dB, and $v = 60$ km/h from the first downlink slot to the seventh slot are shown in Fig. 10 and Fig. 11, respectively.

It can be seen from Fig. 10 that without slot-level channel extrapolation (dotted lines), there are significant estimation errors between the estimated downlink channel at the first downlink slot and the downlink channels at other downlink slots. Therefore, slot-level channel extrapolation is essential to reduce the channel estimation errors for these downlink channels. From Fig. 10, the ‘KDD-SFCEN + TUDCEN’

(the orange solid line) always achieves the best NMSE performance compared with other methods. In addition, the ‘SF-CNN + TUDCEN’ (the azure solid line) also keeps a relatively good extrapolation accuracy, showing that the proposed TUDCEN can also be applied to other uplink channel estimation methods. Compared with the proposed TUDCEN, the performance of the ‘KDD-SFCEN + LSTM’ and ‘SF-CNN + LSTM’ (dashed lines) degrades sharply to a poor NMSE regime at the second slot, indicating that the LSTM-based channel predictor is unable to deal with high-dimensional CSI matrices and provide accurate slot-level channel estimates.

As depicted in Fig. 11, both the ‘KDD-SFCEN + TUDCEN’ and ‘SF-CNN + TUDCEN’ (orange and azure solid lines) achieve a good achievable sum-rate performance at all downlink slots. Specifically, the ‘KDD-SFCEN + TUDCEN’ achieves 89% (at the seventh downlink slot) to 99% (at the first downlink slot) of the upper bound achievable sum-rate obtained with the perfect CSI (the red solid line). It is also worth emphasizing that the worst achievable sum-rate performance obtained by the ‘KDD-SFCEN + TUDCEN’ is near the achievable sum-rate performance that can be obtained by traditional linear spline interpolation and DFT interpolation methods with a small SRS period $T_p = 0.25$ ms (purple and yellow solid lines), demonstrating that with the proposed framework, the pilot signal can be sent less frequently (i.e., $T_p = 1$ ms) while maintaining a satisfying achievable sum-rate performance, thereby further reducing the pilot training overhead by 4 times. In addition, compared with the general pilot training scheme (Fig. 1 (d)), the proposed TUDCEN-based slot-level channel extrapolation-aided pilot training scheme (Fig. 1 (e)) configures more slots for downlink data transmission instead of for uplink channel estimation, thereby significantly improving the system’s spectral efficiency.

VI. CONCLUSION

This paper proposed a spatial, frequency, and temporal channel extrapolation framework for TDD mmWave massive MIMO-OFDM systems to systematically reduce the pilot training overhead under high-mobility scenarios. Specifically, two neural networks, namely the KDD-SFCEN and the TUDCEN, were proposed to reduce the spatial-frequency domain pilot training overhead and to reduce the temporal domain pilot training overhead, respectively. Extensive numerical results demonstrated that the proposed spatial, frequency, and temporal channel extrapolation framework can effectively reduce the spatial-frequency domain pilot training overhead by more than 4 times via spatial-frequency channel extrapolation and further reduce the temporal domain pilot training overhead by additional 4 times and significantly improve the system’s spectral efficiency via enlarging the pilot signal period with slot-level channel extrapolation.

REFERENCES

- [1] E. G. Larsson, O. Edfors, F. Tufvesson, and T. L. Marzetta, “Massive MIMO for next generation wireless systems,” *IEEE Commun. Mag.*, vol. 52, no. 2, pp. 186–195, Feb. 2014.
- [2] J. Feng, S. Ma, S. Aïssa, and M. Xia, “Two-way massive MIMO relaying systems with non-ideal transceivers: Joint power and hardware scaling,” *IEEE Trans. Commun.*, vol. 67, no. 12, pp. 8273–8289, Dec. 2019.
- [3] J. Feng, S. Ma, G. Yang, and H. V. Poor, “Impact of Antenna Correlation on Full-Duplex Two-Way Massive MIMO Relaying Systems,” *IEEE Trans. Wireless Commun.*, vol. 17, no. 6, pp. 3572–3587, Jun. 2018.
- [4] B. Zhou, X. Yang, J. Wang, S. Ma, F. Gao, and G. Yang, “A low-overhead incorporation-extrapolation based few-shot CSI feedback framework for massive MIMO systems,” *arXiv:2312.04062*, Dec. 2023.
- [5] X. Chen, C. Deng, B. Zhou, H. Zhang, G. Yang, and S. Ma, “High-accuracy CSI feedback with super-resolution network for massive MIMO systems,” *IEEE Wireless Commun. Lett.*, vol. 11, no. 1, pp. 141–145, Jan. 2022.
- [6] K. T. Truong and R. W. Heath, “Effects of channel aging in massive MIMO systems,” *J. Commun. Networks*, vol. 15, no. 4, pp. 338–351, Aug. 2013.
- [7] T. L. Marzetta, E. G. Larsson, H. Yang, and H. Q. Ngo, *Fundamentals of Massive MIMO*. Cambridge University Press, 2016.
- [8] X. Lu, Y. Lu, J. Xu, and G. Lin, “Least square channel estimation for MIMO-OFDM system,” in *Proc. WiCom*, Sep. 2009, pp. 1–4.
- [9] Dmitry. V. Kusaykin, D. V. Denisov, and Maxim. A. Klevakin, “Based interpolation channel estimation for millimeter-wave MIMO OFDM systems with multibeam luneburg antenna,” in *Proc. APEIE*, Nov. 2021, pp. 224–227.
- [10] M. Soltani, V. Pourahmadi, A. Mirzaei, and H. Sheikhzadeh, “Deep learning-based channel estimation,” *IEEE Commun. Lett.*, vol. 23, no. 4, pp. 652–655, Apr. 2019.
- [11] B. Zhou, X. Yang, S. Ma, F. Gao, and G. Yang, “Pay less but get more: A dual-attention-based channel estimation network for massive MIMO systems with low-density pilots,” *IEEE Trans. Wireless Commun.*, vol. 23, no. 6, pp. 6061–6076, Jun. 2024.
- [12] B. Lin, F. Gao, S. Zhang, T. Zhou, and A. Alkhateeb, “Deep learning-based antenna selection and CSI extrapolation in massive MIMO systems,” *IEEE Trans. Wireless Commun.*, vol. 20, no. 11, pp. 7669–7681, Nov. 2021.
- [13] Y. Yang, S. Zhang, F. Gao, C. Xu, J. Ma, and O. A. Dobre, “Deep learning based antenna selection for channel extrapolation in FDD massive MIMO,” in *Proc. WCSP*, Oct. 2020, pp. 182–187.
- [14] H. P. Bui, Y. Ogawa, T. Nishimura, and T. Ohgane, “Performance evaluation of a multi-user MIMO system with prediction of time-varying indoor channels,” *IEEE Trans. Antennas Propag.*, vol. 61, no. 1, pp. 371–379, Jan. 2013.
- [15] K. Baddour and N. Beaulieu, “Autoregressive modeling for fading channel simulation,” *IEEE Trans. Wireless Commun.*, vol. 4, no. 4, pp. 1650–1662, Jul. 2005.
- [16] A. Duel-Hallen, “Fading channel prediction for mobile radio adaptive transmission systems,” *Proc. IEEE*, vol. 95, no. 12, pp. 2299–2313, Dec. 2007.
- [17] S. R. Mattu, L. N. Theagarajan, and A. Chockalingam, “Deep channel prediction: A DNN framework for receiver design in time-varying fading channels,” *IEEE Trans. Veh. Technol.*, vol. 71, no. 6, pp. 6439–6453, Jun. 2022.
- [18] H. Jiang, M. Cui, D. W. K. Ng, and L. Dai, “Accurate channel prediction based on transformer: Making mobility negligible,” *IEEE J. Sel. Areas Commun.*, vol. 40, no. 9, pp. 2717–2732, Sep. 2022.
- [19] P. Dong, H. Zhang, G. Y. Li, I. S. Gaspar, and N. NaderiAlizadeh, “Deep CNN-based channel estimation for mmWave massive MIMO systems,” *IEEE J. Sel. Top. Signal Process.*, vol. 13, no. 5, pp. 989–1000, Sep. 2019.
- [20] T. B. Brown, B. Mann, N. Ryder, M. Subbiah, J. Kaplan, P. Dhariwal, A. Neelakantan, P. Shyam, G. Sastry, A. Askell, S. Agarwal, A. Herbert-Voss, G. Krueger, T. Henighan, R. Child, A. Ramesh, D. M. Ziegler, J. Wu, C. Winter, C. Hesse, M. Chen, E. Sigler, M. Litwin, S. Gray, B. Chess, J. Clark, C. Berner, S. McCandlish, A. Radford, I. Sutskever, and D. Amodei, “Language models are few-shot learners,” *arXiv:2005.14165*, Jul. 2020.
- [21] 3GPP, “NR; Physical channels and modulation,” *3GPP, Sophia Antipolis, France, TS 38.211 V17.4.0*, Jan. 2023.
- [22] X. Jiang and F. Kaltenberger, “Channel reciprocity calibration in TDD hybrid beamforming massive MIMO systems,” *IEEE J. Sel. Top. Signal Process.*, vol. 12, no. 3, pp. 422–431, Jun. 2018.
- [23] M. Chen, J. Guo, C.-K. Wen, S. Jin, G. Y. Li, and A. Yang, “Deep learning-based implicit CSI feedback in massive MIMO,” *IEEE Trans. Commun.*, vol. 70, no. 2, pp. 935–950, Feb. 2022.
- [24] K. He, X. Zhang, S. Ren, and J. Sun, “Deep residual learning for image recognition,” in *Proc. IEEE/CVF CVPR*, Jun. 2016, pp. 770–778.
- [25] J. L. Ba, J. R. Kiros, and G. E. Hinton, “Layer normalization,” *arXiv:1607.06450*, Jul. 2016.
- [26] A. Vaswani, N. Shazeer, N. Parmar, J. Uszkoreit, L. Jones, A. N. Gomez, Ł. Kaiser, and I. Polosukhin, “Attention is all you need,” in *Proc. NIPS*, May 2017, pp. 5998–6008.
- [27] N. Srivastava, G. Hinton, A. Krizhevsky, I. Sutskever, and R. Salakhutdinov, “Dropout: A simple way to prevent neural networks from overfitting,” *J. Mach. Learn. Res.*, vol. 15, no. 56, pp. 1929–1958, 2014.
- [28] OpenAI, “Introducing ChatGPT.” [Online]. Available: <https://openai.com/blog/chatgpt>
- [29] MathWorks, “MATLAB 5G toolbox,” Feb. 2023. [Online]. Available: <https://ww2.mathworks.cn/en/products/5g.html>
- [30] 3GPP, “Study on channel model for frequencies from 0.5 to 100 GHz,” *3GPP, Sophia Antipolis, France, TR 38.901 V17.0.0*, Mar. 2022.